Journal of Materials Science: Materials in Electronics (2019) 30:6157–6165
https://doi.org/10.1007/s10854-019-00917-w

Flexible lead-free piezo-/ferroelectric $Bi_{0.5}(Na_{0.6}K_{0.4})_{0.5}TiO_3$ ceramic incorporated PDMS polymer composites for energy harvesting application

Kriti Batra[1] · Nidhi Sinha[2] · Binay Kumar[1]

Received: 16 October 2018 / Accepted: 11 February 2019 / Published online: 19 February 2019

Abstract
Environment friendly piezoelectric micro/nanogenerators have attracted tremendous attention due to the increasing demand of portable self-powered devices. Here, we report the synthesis of $Bi_{0.5}(Na_{0.6}K_{0.4})_{0.5}TiO_3$ (BNKT) ceramic via solid state reaction method and the fabrication of BNKT:PDMS based flexible energy harvester. The synthesized BNKT ceramic exhibits well-defined fatigue free P-E hysteresis loops up to 10^4 cycles favourable for high precision capacitors and sensors. A high value of piezoelectric charge coefficient ($d_{33} = 154$ pC N^{-1}) was measured for BNKT ceramic, which indicates its potential application in flexible energy harvesting devices. A series of flexible BNKT:PDMS composite based microgenerators were fabricated with 10, 20, 30 and 40 wt% BNKT content and their dielectric and electrical properties were investigated. The energy harvester with 40 wt% BNKT achieved the highest dielectric constant and conductivity, whereas the device with 30 wt% BNKT ceramic generated the highest open circuit voltage of about 11 V under periodic compressive force of 20 N. These results imply that lead free BNKT:PDMS composite may be applied in pressure sensors and various energy harvesting devices.

1 Introduction

Energy harvesting from piezoelectric materials has attracted considerable attention as an eco-friendly way to scavenge energy from immediate environment, thereby solving the serious problem of energy shortage [1–3]. Mechanical energy sources like flowing air, sound waves, human motions, mechanical impacts etc. are abundant in our living surrounding and can be converted into electrical energy via piezoelectric nano/microgenerators employing piezoelectric materials. Many researchers have demonstrated the ability of piezoelectric materials such as ZnO, $BaTiO_3$, PZT, GaN, $ZnSnO_3$, PMN-PT, NKLN etc. for powering wireless sensors, implantable biomedical devices and portable electronic devices [4–16]. For example, Lai et al. have demonstrated the application of ZnO based PENG as self-powered gas sensors [4]. Lee et al. presented a nanogenerator that can scavenge energy from skin wrinkling [12]. Piezoelectric energy harvesters have been successfully utilized for powering small electronic devices [17, 18].

Intensive efforts have been made by the researchers to boost the output performance of piezoelectric generator. The most effective way to achieve high output voltage/current from the flexible piezoelectric energy harvesters is to adopt ferroelectric materials with high electromechanical coefficient [19, 20]. The ABO_3 oxide perovskites are interesting candidates for energy harvesting applications due to their efficient piezoelectric and ferroelectric properties [7, 21–24]. The conventional perovskite compounds such as PZT, PMN-PT, PZN-PT and various other lead based materials shows excellent piezoelectric, pyroelectric and ferroelectric properties [20, 25–28]. However, these materials contain lead oxide in high level (more than 60%) which gives rise to ecological pollution due to its toxicity. Therefore, the lead free piezoelectric materials having high electromechanical coefficient (d_{33} value) would be desirable for flexible energy harvesting devices [15, 29–31].

Alkali-based lead free piezoelectric perovskite materials such as sodium bismuth titanate (NBT), potassium sodium niobate (KNN) and potassium bismuth titanate

✉ Binay Kumar
b3kumar69@yahoo.co.in

[1] Crystal Lab, Department of Physics & Astrophysics, University of Delhi, Delhi 110007, India

[2] Department of Electronics, SGTB Khalsa College, University of Delhi, Delhi 110007, India

(KBT) are the potential alternatives to lead-based piezoelectric materials [32–35]. NBT is a promising candidate for lead free piezoelectric material which exhibits large remnant polarization of ~ 37 μC cm^{-2} and high Curie temperature ~ 320 °C but suffers from problems in poling process due to high conductivity and coercive field. In past, several studies have been carried out to enhance the piezoelectric properties of NBT by adding another perovskite solid solutions such as $Na_{0.5}Bi_{0.5}TiO_3$–$K_{0.5}Bi_{0.5}TiO_3$ (i.e. NBT-KBT), $Na_{0.5}Bi_{0.5}TiO_3$–$NaNbO_3$ (i.e. NBT-NN), $Na_{0.5}Bi_{0.5}TiO_3$–$SrTiO_3$ (i.e. NBT-ST) and $Na_{0.5}Bi_{0.5}TiO_3$–$K_{0.5}Bi_{0.5}TiO_3$–$BaTiO_3$ (i.e. NBT-KBT-BT) [36–38]. Among various NBT based ceramic systems, $(1-x)$ NBT-x KBT binary system possess excellent dielectric and piezoelectric properties in the vicinity of rhombohedral–tetragonal morphotropic phase boundary region (i.e. $0.16 \le x \le 0.20$) [35, 39]. Yang et al. investigated the structural and piezoelectric properties of $(1-x)$ $Bi_{0.5}Na_{0.5}TiO_3$ − x $Bi_{0.5}$ $K_{0.5}TiO_3$ ceramics in the range $0.16 \le x \le 0.20$ and found the maximum d_{33} value (144 pC N^{-1}) at $x = 0.18$ [35]. However, due to instability issues associated with compositions near MPB, researchers are now focussing on compositions far away from MPB [40–42]. Kumar and co-workers synthesized $Bi_{0.5}(Na_{0.5}K_{0.5})_{0.5}TiO_3$ ceramic and achieved a high d_{33} value equal to 115 pC N^{-1} [41]. A piezoelectric charge coefficient (d_{33}) value of ~ 132 pC N^{-1} was reported by Bhandari et al. for $Bi_{0.5}(Na_{0.65}K_{0.35})_{0.5}TiO_3$ ceramics [43].

PDMS is widely used polymer for fabrication of various devices because of its attractive properties such as biocompatibility, flexibility, water resistance, cost effectiveness and chemical stability [15, 44]. Also, because of low dielectric constant and stiffness coefficient, PDMS polymer can be combined with the piezoelectric ceramic materials with high dielectric permittivity [44, 45].

In this work, we first report the synthesis of $Bi_{0.5}(Na_{0.6}K_{0.4})_{0.5}TiO_3$ (BNKT) ceramic via solid state reaction route with fairly high d_{33} ~ 154 pC N^{-1}. The flexible energy harvesters based on BNKT ceramic and PDMS polymer with different contents of BNKT (10–40 wt%) were then fabricated. The microgenerator was fabricated by spin coating a mixture of BNKT ceramic and PDMS polymer on ITO coated PET substrate. The dielectric properties and AC conductivity of the composite based energy harvesting devices with different BNKT contents were then investigated. The output voltage signals of the fabricated composite based piezoelectric microgenerators (PMGs) were measured under compressive stress. The microgenerator with 30 wt% BNKT showed highest output voltage signal. This BNKT:PDMS energy harvester (30 wt%) produced high output voltage of about 11 V when subjected to periodic vertical compressive force of 20 N.

2 Experimental details

2.1 Synthesis of BNKT ceramic

BNKT ceramic was synthesized via solid state reaction method, using bismuth oxide, titanium dioxide, sodium carbonate and potassium carbonate from Sigma Aldrich (> 99% purity) as starting ingredients. The powders were mixed homogeneously and ground using ball mill for 12 h followed by calcination at 850 °C for 10 h. The resulting powder was pressed into pellets (12 mm diameter) after adding 2 wt% polyvinyl alcohol (binder) under a pressure of 100 MPa. The pellets were first kept at 650 °C to burn the binder and then sintered at 1050 °C for 3 h. The sintered pellets were crushed and ground to powder using ball mill for 10 h.

2.2 Fabrication of BNKT ceramic based energy harvester

The schematic process involved in the fabrication of PMG is illustrated in Fig. 1. To fabricate BNKT ceramic based flexible piezoelectric energy harvester, polydimethylsiloxane (PDMS) polymer solution was prepared by adding curing agent to base PDMS material (1:10 weight ratio). The as-prepared BNKT ceramic was dispersed into PDMS solution at different concentrations of 10, 20, 30 and 40 wt % with the help of magnetic stirrer (Fig. 1b). The resultant composite mixture was spin coated onto an ITO coated polyethylene terephthalate (PET) substrate at a spinning rate of 600 rpm for 30 s followed by curing at 60 °C for 2 h (Fig. 1c).

ITO/PET substrate was chosen as flexible conducting electrode for the device because of its low electrical resistance and chemical stability. Next, aluminium (Al) coated polyethersulfone (PES) substrate (top electrode) was mechanically integrated with the composite layer (Fig. 1d)

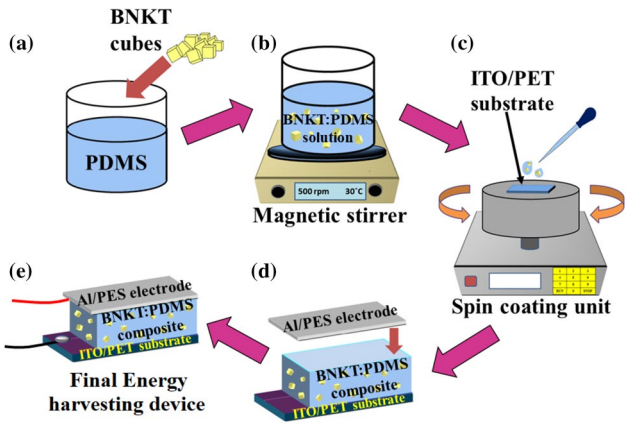

Fig. 1 Schematic diagram showing the fabrication process of flexible BNKT ceramic based energy harvester

and final device (after connecting copper wires to the electrodes by silver paste) was coated by PDMS to keep the device robust under applied mechanical stress. The final structure of energy harvesting device is shown in Fig. 1e. The effective size of all BNKT based devices was about 2 cm × 2 cm each.

2.3 Characterization techniques

The structural and crystallographic characterizations of BNKT ceramic were studied using XRD (Rigaku Ultima IV X-ray diffractometer) with Cu K_α radiation of wavelength 1.5405 Å. The morphology and the dimensions of the samples were observed by using scanning electron microscope (SEM, Model: EVO MA 10, Zeiss) and field emission scanning electron microscope (FE-SEM, Model: GeminiSEM 500, Zeiss). Ferroelectric P-E hysteresis loop of BNKT sample was traced using PE loop tracer. The pelletized sample of BNKT ceramic was poled electrically at 35 kV cm^{-1} using DC poling unit (Marine India). Piezoelectric charge coefficient (d_{33}) of BNKT ceramic was measured using Piezometer system (Piezotest PM300, UK) at a tapping force of 0.25 N (tapping frequency = 110 Hz). The frequency dependent AC conductivity and dielectric measurements of the samples were carried out at room temperature (RT) using Impedance Analyzer (C-50 alpha A, Novocontrole). An electrodynamic vibration test system (Pacific dynamics) consisting of cylindrical pushing tip of diameter 4.5 mm was used to apply periodic vertical mechanical force (shock) to the device and the force exerted on the device was obtained using computer interface load cell (force sensor, model: 20210, ADI Artech Transducers Pvt. Ltd., India). The piezoelectric performance of the energy harvesters was measured in terms of open circuit voltage using digital storage oscilloscope (DSO, Rigol DSSC06) under vertical compressive force of 20 N (applied pressure ~ 1.2 MPa) after 24 h after poling the device by applying an electric field (DC) of 40 kV cm^{-1} for 12 h.

3 Results and discussions

3.1 Structural and micro structural analysis

The powder X-ray diffraction pattern of BNKT ceramic calcined at 850 °C and sintered at 1050 °C is represented in Fig. 2a. XRD pattern of sintered BNKT indicates perovskite structure of BNKT with good crystallinity and is in accordance with JCPDS card No. 98-009-8049 assigned for BNKT (Tetragonal symmetry). Furthermore, no peaks corresponding to pyrochlore phase were found in the recorded diffraction pattern. Rietveld refinement of powder XRD data was carried out using Topas software (Fig. 2b). The lattice parameters were determined to be a = b = 3.8979 Å and c = 3.8898 Å having tetragonal crystal structure and P4mm symmetry. The refinement parameters were found to be: $R_p = 9.21$, $R_{wp} = 11.73$, $R_{exp} = 10.09$, and GOF = 1.16.

The morphology and the dimensions of as synthesized BNKT sample were investigated using SEM. Figure 3a shows the SEM image of sintered pellet of BNKT powder exhibiting cubic morphology with the side length in the range 87 nm to 0.44 µm. A statistical distribution of the side length of BNKT microcubes through the entire sample is depicted in Fig. 3b and the average cube size was found to be 0.268 µm.

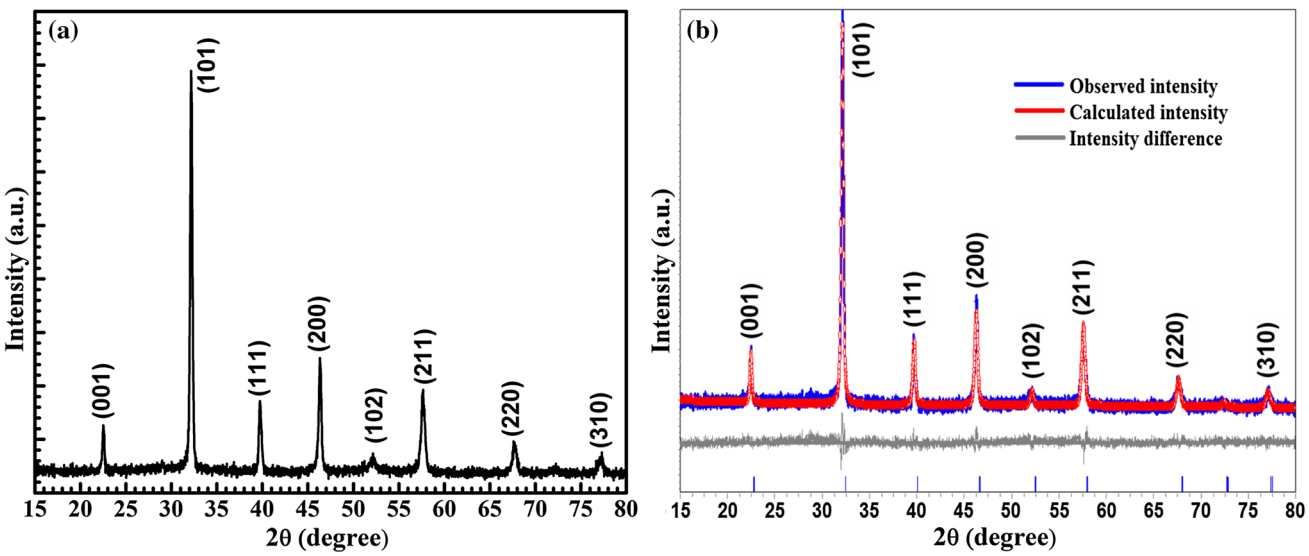

Fig. 2 **a** Powder XRD pattern of BNKT ceramic. **b** XRD profile fit for BNKT ceramic

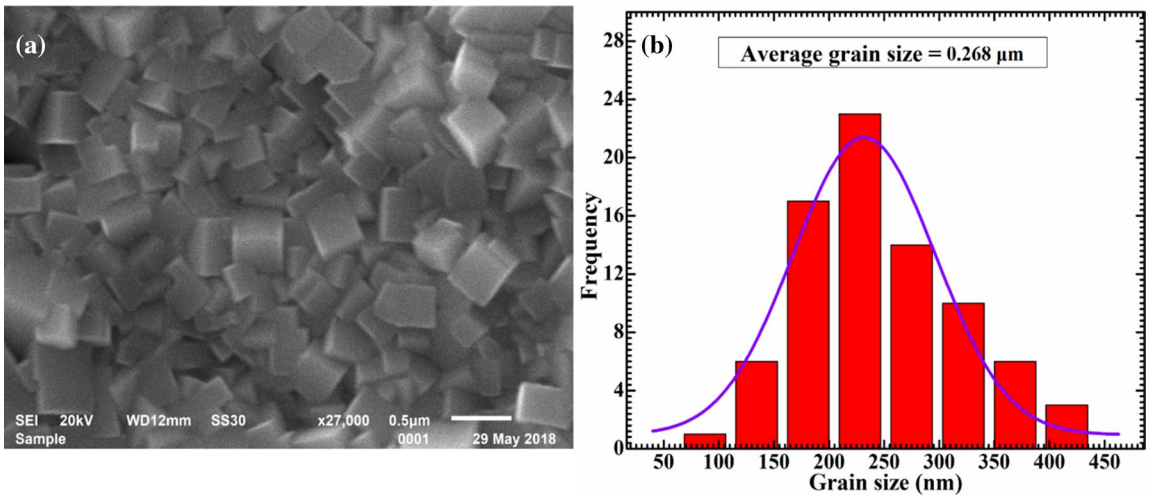

Fig. 3 **a** SEM image of BNKT powder pellet sintered at 1050 °C. **b** Histogram showing grain size distribution of BNKT microcubes with an average grain size of 0.268 µm

The photographic image of BNKT:PDMS (30 wt% of BNKT) composite on ITO/PET substrate prepared by spin coating a mixture of BNKT microcubes and PDMS polymer during bending is shown in Fig. 4a to demonstrate the flexibility of microgenerator. The FESEM images of top (Fig. 4b, c) and bottom (inset of Fig. 4b) surface shows the random, but nearly uniform distribution of BNKT microcubes within the PDMS polymer matrix in both sides. As

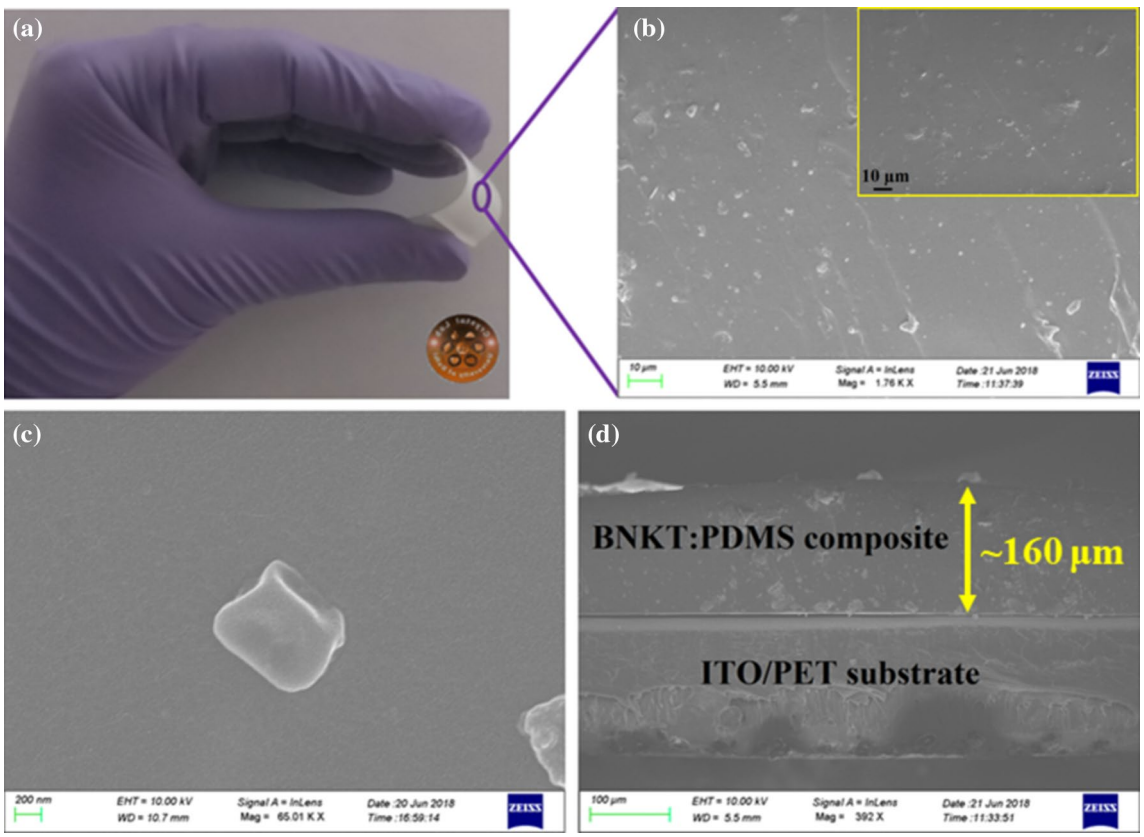

Fig. 4 **a** Photographic image of flexible BNKT:PDMS composite film on transparent ITO/PET substrate. **b** FESEM image of top and bottom (inset) surface of BNKT:PDMS composite film set. **c** High resolution FESEM image of single BNKT microcube in PDMS polymer matrix. **d** A cross-sectional FESEM image of BNKT:PDMS layer on ITO/PET substrate

can be seen, BNKT microcubes are randomly distributed within the PDMS polymer matrix with slightly higher density at the bottom. The thickness of the BNKT:PDMS composite film was estimated to be about 160 µm from the cross-sectional FESEM image (Fig. 4d).

3.2 Piezoelectric and ferroelectric studies of BNKT ceramic

The piezoelectric behaviour of BNKT ceramic was investigated using piezometer at RT. The domains within the microcubes are randomly oriented which can be aligned in the direction of applied field by electric poling. Therefore, the BNKT powder pellets were subjected to electric poling by applying dc field (35 kV cm^{-1}) at RT. The piezoelectric charge coefficient (d_{33}) was measured to be 154 pC N^{-1}, which is much higher than reported values for other perovskite lead-free materials [7, 13, 32, 33]. The observed value of d_{33} is also higher than the values obtained by Zheng et al. and Bhandari et al. for same system but different compositions ($Bi_{0.5}(Na_{0.84}K_{0.16})_{0.5}TiO_3$ and $Bi_{0.5}(Na_{0.65}K_{0.35})_{0.5}TiO_3$, respectively) [42, 43]. The large piezoelectric response for BNKT makes it a potential candidate for various energy harvesting applications.

The existence of ferroelectricity in a sample can be confirmed by measuring polarization as a function of electric field. Figure 5a depicts the P-E hysteresis loops for BNKT microcubes traced at room temperature. As can be seen, BNKT display well shaped and symmetric hysteresis loop thereby confirming ferroelectric behaviour. The values of the coercive field (E_c) and remnant polarization (P_r) were measured to be 23.54 kV cm^{-1} and 22.12 µC cm^{-2}, respectively. For device applications, the long term reliability of ferroelectric properties is very important. Figure 5b shows the fatigue behaviour of BNKT ceramic investigated over 10,000 switching cycles. No significant change was observed in the ferroelectric properties, indicating fatigue resistant behaviour suitable for high precision electromechanical transducers and actuators.

3.3 Dielectric and AC conductivity analysis

Figure 6 shows the frequency dependence of dielectric constant and dielectric loss for BNKT:PDMS composite films with different BNKT contents. The dielectric constant (ε′) was observed to decrease with increase in frequency (from 10 Hz to 2 MHz) for all samples (Fig. 6a). This is due to fact that all the four polarizations (i.e., space charge, electronic, dipolar and ionic) contribute to permittivity at low frequency and the space charge contribution (which is the dominant contribution) diminishes at high frequencies. Moreover, the dielectric constant was found to increase with increasing BNKT loadings. This enhancement is attributed to the high dielectric constant of BNKT ceramic (1663 at 1 KHz, Fig. 6b) as compared to that of pure PDMS polymer (2.5) [46].

Dielectric loss of a material is the proportion of energy dissipated to that stored by polarization in a dielectric under the application of alternating electric field. The variation of dielectric loss with frequency is depicted in Fig. 6c, which demonstrates a gradual decrease of loss tangent with increasing frequency for all composite films. A significant rise in the value of dielectric loss has been observed for the composites with increasing BNKT content, which is due to leakage caused by higher BNKT contents with high electrical conductivity. These results are in agreement with those obtained for other ceramic-polymer composites [47–49]. The low value of dielectric loss (tan δ ~ 0.01 @ RT, 1 kHz for 30 wt% BNKT:PDMS) is preferred for dielectric and piezoelectric applications.

The variation of ac conductivity of BNKT:PDMS composite films as a function of frequency is illustrated in Fig. 6d. The ac conductivity (σ_{ac}) was calculated from the dielectric data using the relation,

$$\sigma_{ac} = \omega \tan\delta \, \varepsilon_o \varepsilon'$$

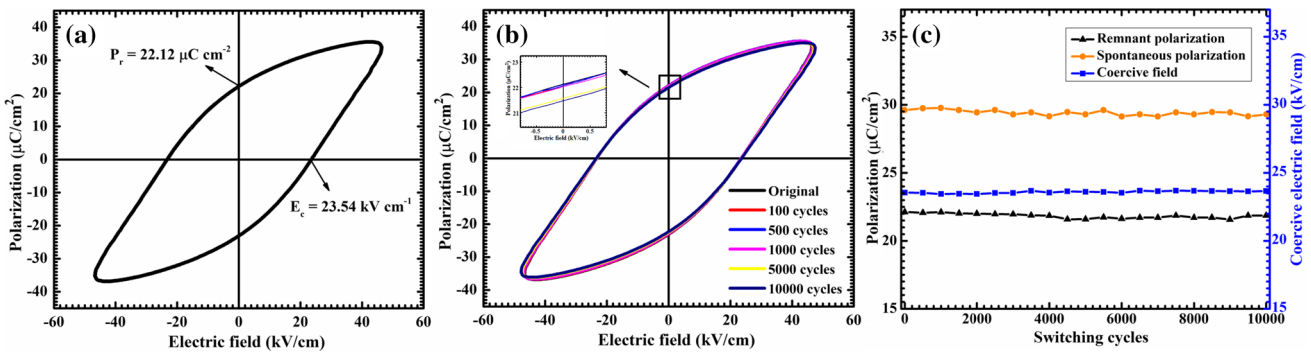

Fig. 5 **a** Ferroelectric P-E hysteresis loop of BNKT ceramic. **b** P-E response for fatigue after various switching cycles. **c** Fatigue analysis plot of BNKT showing remnant polarization, spontaneous polarization and coercive field as a function of switching cycles

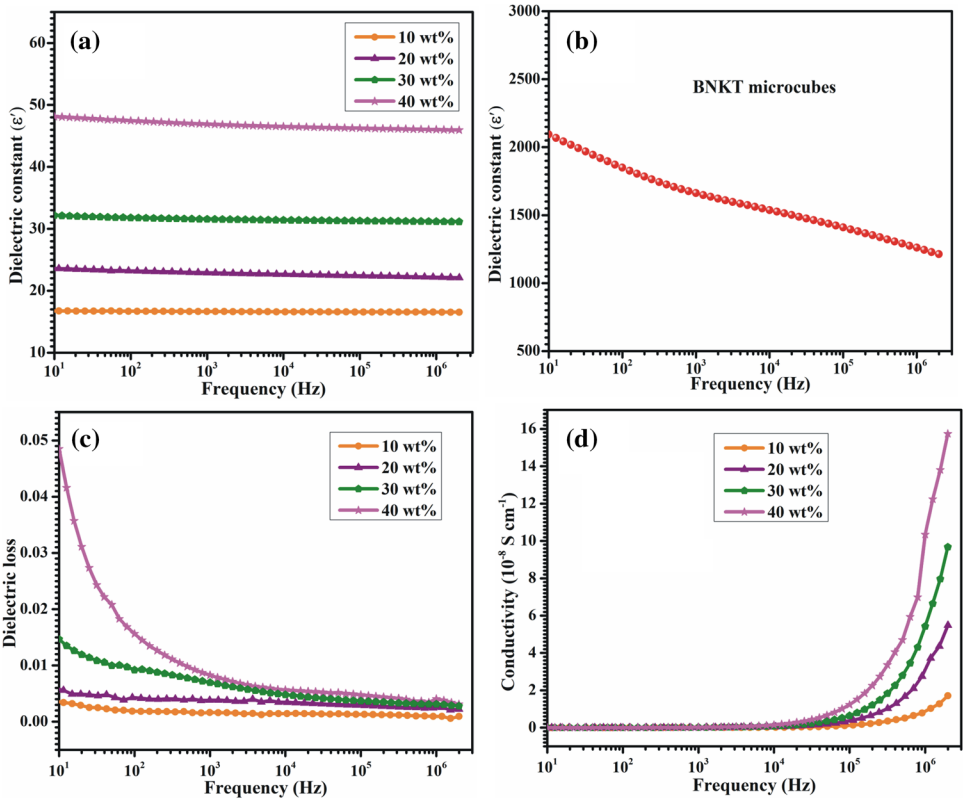

Fig. 6 Dielectric constant of **a** BNKT:PDMS composites with different BNKT contents (10–40 wt%) and **b** BNKT ceramic as a function of frequency. Variation of **c** dielectric loss and **d** AC conductivity with frequency for various BNKT:PDMS composite films

where, ω denotes the angular frequency of the applied field, tanδ is the dielectric loss, ε_o is the vacuum permittivity and ε′ is the real dielectric constant. AC conductivity was found to be frequency independent in low frequency range (1 Hz to 1 KHz) and increases sharply beyond 1 KHz. The flat behaviour at low frequency is attributed to the dc conductivity. The frequency dependence of conductivity can be estimated using Jonscher's power law,

$$\sigma_{ac} = \sigma_{dc} + A\omega^{s}$$

where, σ_{dc} denotes dc conductivity, A is a constant and s is frequency exponent [50]. The value of exponent 's' was found to be between 0.89 and 0.94 for all composites after fitting the power law, which corresponds to hopping conduction mechanism [51].

Also, the AC conductivity of the composite films increased continuously with the increment of BNKT microcubes content leading to reduction in insulating behaviour. The increase in AC conductivity with increasing BNKT content is due to the enhancement in the contribution of interface conductivity between BNKT microcubes and PDMS polymer [52].

3.4 Energy harvesting performance

The detailed information about the piezoelectric microgenerator fabrication process is given in the experimental section. In the piezoelectric microgenerator, BNKT microcubes act as power generation sources and PDMS polymer provides flexibility to energy harvester. In order to study the influence of BNKT microcubes concentration on the output performance of the device, a series of piezoelectric microgenerators with 10, 20, 30 and 40 wt% BNKT microcubes were fabricated and their performance was compared as a function of BNKT content. The piezoelectric output voltage from the BNKT based energy harvesting devices (with 30 wt% BNKT) was measured under periodic vertical compressing and releasing conditions (20 N) using Electrodynamic vibration test system after poling the device with a dc electric field of 40 kV cm^{-1} for 12 h at RT. The generated output voltages from various BNKT energy harvesting devices are shown in Fig. 7. The open circuit output voltage of the piezoelectric microgenerator was observed to increase with increasing BNKT content up to 30 wt% in the polymer matrix and decreased to low value for the energy harvester with higher weight ratio (40 wt%) of BNKT. The drop in the output voltage generated from device with 40 wt% content of BNKT is attributed to its high conductivity leading to weak insulating behaviour of the composite and non-uniform dispersion of BNKT microcubes in PDMS. Therefore, the optimum weight ratio of BNKT was found to be 30 wt%. A large output voltage of about 11 V was obtained from the energy harvesting device (with 30 wt% BNKT) upon periodic vertical compression of 20 N.

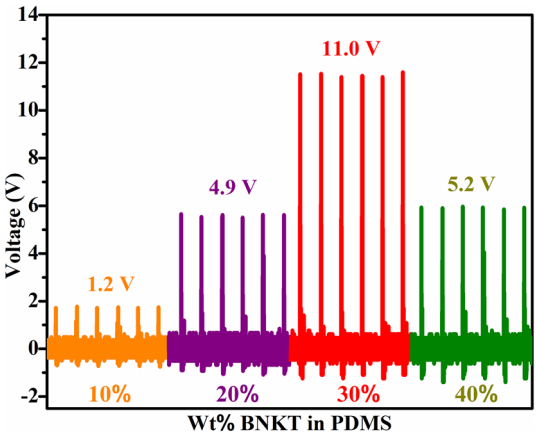

Fig. 7 Output voltage of piezoelectric microgenerators with different BNKT contents (10–40 wt%) under compressive force of 20 N

To check whether the measured signal is arising from BNKT:PDMS device, switching polarity test was carried out for BNKT:PDMS microgenerator by reversing the electrode connection. The generated output voltages from the device in forward and reverse connection under periodic 20 N vertical compressive force are shown in Fig. 8 a–d. An opposite signal is detected when the power generation device is connected in reverse, thereby confirming that the output signals recorded from the device are generated as a result of piezoelectric phenomenon and not by any environmental noise. The magnitude of peak value of output voltage generated during press and release states was observed to be unequal due to different straining rate during application and removal of stress from the power generator.

The piezoelectric voltage generation mechanism from BNKT based microgenerator can be explained as follows. In the absence of any external force (stress/ electric field), electric dipoles within each BNKT microcube are randomly aligned leading to zero net dipole moment and hence no electric output. When the device is poled, the electric dipoles within BNKT microcubes are aligned along the direction of applied electric field. However, no output signal will be detected in the absence of external force due to device being in equilibrium state. Further, when the compressive stress is vertically applied, opposite charges are generated on the top and bottom electrode of the device resulting in the generation of piezoelectric potential. Further, when the applied vertical stress is released, the generated piezoelectric potential disappears causing the charges to move back in opposite direction. Therefore, AC type output signal was generated corresponding to the application and release of compressive force.

A stability test was carried out under periodic vertical compression of 20 N at a frequency of 1 Hz over 700 cycles

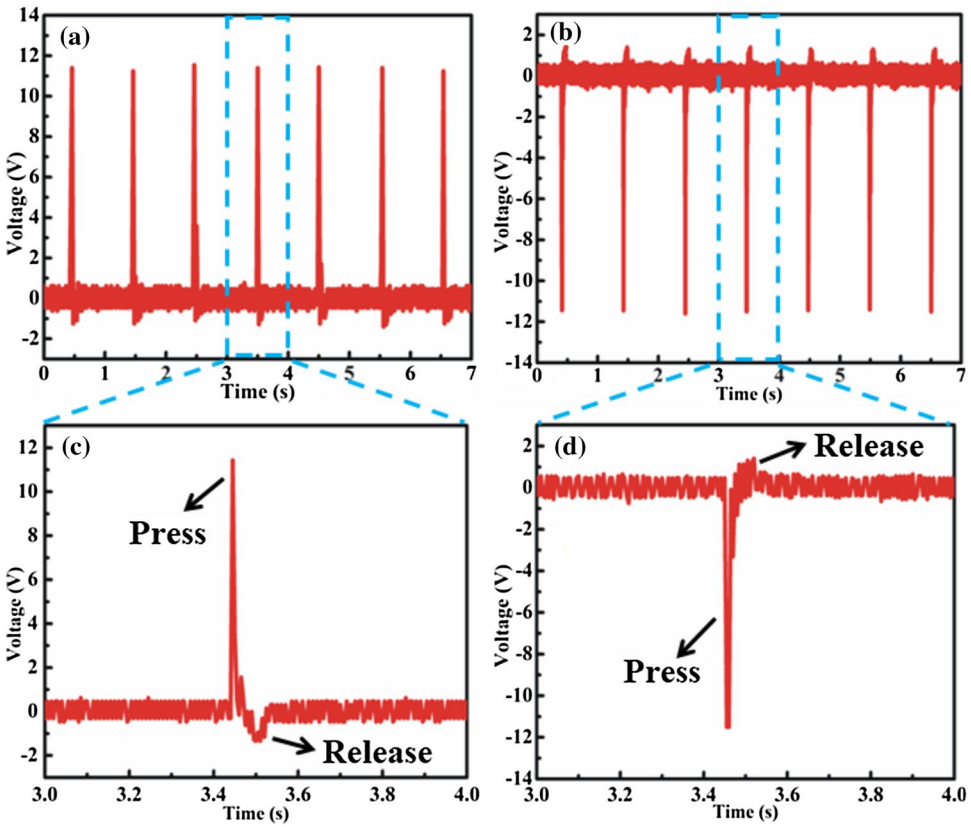

Fig. 8 Piezoelectric output voltage generated from the fabricated energy harvester under vertical compression of 20 N in **a** forward connection and **b** reverse connection. Enlarged view of one cycle of generated output voltage under **c** forward connection and **d** reverse connection

(700 s). As shown in Fig. 9, no degradation in the piezoelectric output performance was observed over the entire period of testing, thereby indicating the excellent stability and reliability of BNKT:PDMS energy harvester.

The energy harvesting performance of various piezoelectric energy harvesters based on perovskite materials and the details of experimental conditions are summarized in Table 1. It can be clearly seen that the fabricated BNKT:PDMS energy harvester exhibits better performance as compared to various previously reported piezoelectric energy harvesters.

The piezoelectric output voltage from the piezoelectric energy harvesting device is influenced by piezoelectric charge coefficient of the material and the dielectric constant of the composite according to relation: $V = \frac{d_{33}\varepsilon Y}{\varepsilon_o K}$, where d_{33} is the piezoelectric charge coefficient, ε is the strain, Y is the Young's modulus of the material, ε_o is the vacuum permittivity and K is the dielectric constant [15]. From the dielectric study, it has been observed that the value of the dielectric constant of composite with 30 wt% BNKT (32 at 1 KHz) is much smaller as compared to BNKT ceramic (1663 at 1 KHz) due to small value of dielectric constant of pure PDMS [42]. Therefore, high d_{33} value of BNKT ceramic and low dielectric constant of BNKT:PDMS composite are responsible for observed large output voltage from the BNKT:PDMS piezoelectric microgenerator.

4 Conclusions

In summary, BNKT microcubes were successfully synthesized through solid state reaction method and characterized as promising candidate for piezoelectric energy harvester due to its high piezoelectric coefficient (154 pC N^{-1}). Composite based flexible microgenerators were then fabricated using the as-synthesized BNKT microcubes and PDMS polymer. The effects of BNKT microcubes (10–40 wt%) on the dielectric and electrical properties were evaluated. Both dielectric constant and AC conductivity were found to increase with increasing BNKT content. The piezoelectric microgenerator with 30 wt% of BNKT generated the highest output voltage of ~ 11 V under vertical compression of 20 N. Observed high output voltage from the device was explained in terms of high d_{33} value of BNKT microcubes and low dielectric constant of BNKT:PDMS composite. Our work indicates that BNKT based microgenerator can be realized to scavenge energy from human body motion for powering wireless electronics and various self-powered devices.

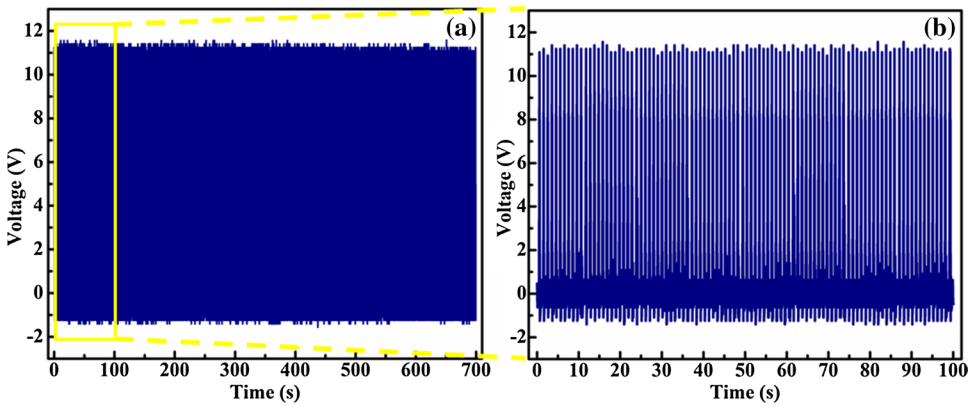

Fig. 9 **a** Stability test of BNKT:PDMS energy harvester under vertical compressive force of 20 N. **b** Enlarged view of output voltage signals for 100 cycles

Table 1 Comparison of the energy harvesting performance of BNKT:PDMS based energy harvester with other reported data

Composite piezoelectric energy harvester	Thickness of composite layer (μm)	Area of NG (cm^2)	Poling conditions	Working mode	Output voltage (V)	Reference
$BaTiO_3$:PDMS	300	1.0	80 kV/cm, 12 h	Compressive force of 1 MPa	5.5	7
$BiFeO_3$:PDMS	100	2.5	200 kV/cm, 10 h, 150 °C	Repeating hand impacting	3.0	9
PMN-PT:PDMS	150	0.5	50 kV/cm, 24 h, 150 °C	Tapping using plastic handle of screw driver	7.8	14
$KNbO_3$:PDMS	25	7.2	150 kV/cm, 1 h, RT	Compressive strain of 0.38%	3.2	21
$LiNbO_3$:PDMS	350	6.0	90 kV/cm, RT	Compressive force of 1 kgf	4.0	23
$NaNbO_3$:PDMS	100	4.5	80 kV/cm, RT	Compressive strain of 0.23%	3.2	24
BNKT:PDMS	160	4.0	40 kV/cm, 12 h, RT	Compressive force of 20 N	11.0	Present work

Acknowledgements This work was financially supported by grant received through the DST Project (EMR/2015/000385) and DRDO Project (ARMREB/MAA/2015/163). Kriti Batra would like to thank DST for providing Junior Research Fellowship (JRF). Dr. Nidhi Sinha is thankful to the Principal, SGTB Khalsa College for continuous motivation and support for research work.

Compliance with ethical standards

Conflict of interest The authors declare no conflict of interest.

References

1. K.Y. Lee, M.K. Gupta, S.-W. Kim, Nano Energy **14**, 139 (2015)
2. S. Xu, Y. Qin, C. Xu, Y. Wei, R. Yang, Z.L. Wang, Nat. Nanotechnol. **5**, 366 (2010)
3. S.R. Anton, H.A. Sodano, Smart Mater. Struct. **16**, R1 (2007)
4. Y. Zhao, X. Lai, P. Deng, Y. Nie, Y. Zhang, L. Xing, X. Xue, Nanotechnology **25**, 115502 (2014)
5. K. Batra, N. Sinha, S. Goel, H. Yadav, A.J. Joseph, B. Kumar, J. Alloys Compd. **767**, 1003 (2018)
6. N. Sinha, S. Goel, A.J. Joseph, H. Yadav, K. Batra, M.K. Gupta, B. Kumar, Ceram. Int. **44**, 8582 (2018)
7. Z.-H. Lin, Y. Yang, J.M. Wu, Y. Liu, F. Zhang, Z.L. Wang, J. Phys. Chem. Lett. **3**, 3599 (2012)
8. C. Luo, S. Hu, M. Xia, P. Li, J. Hu, G. Li, H. Jiang, W. Zhang, Energy Technol. **6**, 922 (2018)
9. X. Ren, H. Fan, Y. Zhao, Z. Liu, ACS Appl. Mater. Interfaces **8**, 26190 (2016)
10. T. Dufay, B. Guiffard, R. Seveno, J.-C. Thomas, Energy Technol. **6**, 917 (2018)
11. M. Johar, M. Hassan, A. Waseem, J.-S. Ha, J. Lee, S.-W. Ryu, Nanomaterials **8**, 437 (2018)
12. S. Lee, S. Bae, L. Lin, Y. Yang, C. Park, S.-W. Kim, S.N. Cha, H. Kim, Y.J. Park, Z.L. Wang, Adv. Funct. Mater. **23**, 2445 (2013)
13. K.Y. Lee, D. Kim, J.-H. Lee, T.Y. Kim, M.K. Gupta, S.-W. Kim, Adv. Funct. Mater. **24**, 37 (2014)
14. S. Xu, Y. Yeh, G. Poirier, M.C. McAlpine, R.A. Register, N. Yao, Nano Lett. **13**, 2393 (2013)
15. M.K. Gupta, S. Kim, B. Kumar, ACS Appl. Mater. Interfaces **8**, 1766 (2016)
16. V.L. Stuber, D.B. Deutz, J. Bennett, D. Cannel, D.M. de Leeuw, S. van der Zwaag, P. Groen, Energy Technol. **7**, 177 (2019)
17. Z.L. Wang, G. Zhu, Y. Yang, S. Wang, C. Pan, Mater. Today **15**, 532 (2012)
18. X. Pu, W. Hu, Z.L. Wang, Small **14**, 1702817 (2018)
19. R. Zhu, J. Jiang, Z. Wang, Z. Cheng, H. Kimura, RSC Adv. **6**, 66451 (2016)
20. S. Xu, G. Poirier, N. Yao, Nano Lett. **12**, 2238 (2012)
21. J.H. Jung, C. Chen, B.K. Yun, N. Lee, Y. Zhou, W. Jo, L.-J. Chou, Z.L. Wang, Nanotechnology **23**, 375401 (2012)
22. K. Terada, T. Suzuki, I. Kanno, H. Kotera, Vacuum **81**, 571 (2007)
23. M.K. Gupta, J. Aneesh, R. Yadav, K.V. Adarsh, S.-W. Kim, J. Appl. Phys. **121**, 175103 (2017)
24. J.H. Jung, M. Lee, J.-I. Hong, Y. Ding, C.-Y. Chen, L.-J. Chou, Z.L. Wang, ACS Nano **5**, 10041 (2011)
25. S. Samanta, V. Sankaranarayanan, K. Sethupathi, Vacuum **156**, 456 (2018)
26. A. Hussain, N. Sinha, S. Bhandari, H. Yadav, B. Kumar, J. Asian Ceram. Soc. **4**, 337 (2016)
27. A.K. Singh, K. Kumar, M.K. Gupta, B. Kumar, Phys. Status Solidi **207**, 2564 (2010)
28. A. He, X. Li, Z. Wang, X. Long, S. Mao, Z. Ye, Chem. Mater. **22**, 5588 (2010)
29. I. Coondoo, N. Panwar, D. Alikin, I. Bdikin, S.S. Islam, A. Turygin, V.Y. Shur, A.L. Kholkin, Acta Mater. **155**, 331 (2018)
30. R. Rianyoi, R. Potong, A. Ngamjarurojana, A. Chaipanich, J. Mater. Sci. **53**, 345 (2018)
31. A. Patra, A. Sasmal, A. Seal, S. Sen, J. Mater. Sci. Mater. Electron. **29**, 14046 (2018)
32. I. Roleder, I. Franke, A.M. Glazer, P.A. Thomas, S. Miga, J. Suchanicz, J. Phys. Condens. Matter **14**, 314 (2002)
33. I. Wu, J.L. Zhang, C.L. Wang, J.C. Li, J. Appl. Phys. **103**, 084116 (2008)
34. P.K. Panda, J. Mater. Sci. **44**, 5049 (2009)
35. Z. Yang, B. Liu, L. Wei, Y. Hou, Mater. Res. Bull. **43**, 81 (2008)
36. Y. Li, W. Chen, J. Zhou, Q. Xu, H. Sun, R. Xu, Mater. Sci. Eng. B **112**, 5 (2004)
37. J.R. Gomah-Pettry, A.N. Salak, P. Marchet, V.M. Ferreira, J.P. Mercurio, Phys. Status Solidi **241**, 1949 (2004)
38. W. Chen, Y. Li, Q. Xu, J. Zhou, J. Electroceramics **15**, 229 (2005)
39. G.-H. Lee, Y.-H. Kwon, J.-H. Koh, Ceram. Int. **41**, 7897 (2015)
40. S.-E.E. Park, W. Hackenberger, Curr. Opin. Solid State Mater. Sci. **6**, 11 (2002)
41. I. Kumar, B.K. Singh, M.K. Gupta, N. Sinha, B. Kumar, Ceram. Int. **37**, 2997 (2011)
42. Q. Zheng, J. Ma, D. Lin, J. Mater. Sci. Mater. Electron. **24**, 3836 (2013)
43. S. Bhandari, N. Sinha, G. Ray, B. Kumar, Scr. Mater. **89**, 61 (2014)
44. I.M. Alam, D. Mandal, ACS Appl. Mater. Interfaces **8**, 1555 (2016)
45. K. Sappati, S. Bhadra, Sensors **18**, 3605 (2018)
46. I. Molberg, Y. Leterrier, C.J.G. Plummer, C. Walder, C. Löwe, D.M. Opris, F.A. Nüesch, S. Bauer, J.-A.E. Månson, J. Appl. Phys. **106**, 054112 (2009)
47. U. Yaqoob, A.S.M.I. Uddin, G.-S. Chung, Compos. Part B Eng. **136**, 92 (2018)
48. J. Yan, Y.G. Jeong, Compos. Sci. Technol. **144**, 1 (2017)
49. S. Das, A.K. Biswal, K. Parida, R.N.P. Choudhary, A. Roy, Appl. Surf. Sci. **428**, 356 (2018)
50. A.K. Jonscher, J. Mater. Sci. **16**, 2037 (1981)
51. G. Ray, N. Sinha, B. Kumar, Mater. Chem. Phys. **142**, 619 (2013)
52. I. Babu, G. de With, Compos. Sci. Technol. **91**, 91 (2014)